

Model for diffusion at the microcanonical superheating limit from atomistic computer simulationsSergio Davis,^{1,2} Anatoly B. Belonoshko,³ Börje Johansson,^{4,5} and Anders Rosengren³¹*Grupo de Nanomateriales, Departamento de Física, Facultad de Ciencias, Universidad de Chile, Casilla 653, Santiago, Chile*²*Applied Materials Physics, Department of Materials Science and Engineering, KTH, SE-100 44 Stockholm, Sweden*³*Condensed Matter Theory, Department of Theoretical Physics, AlbaNova University Center, KTH, SE-106 91 Stockholm, Sweden*⁴*Applied Materials Physics, Department of Materials Science and Engineering, KTH, SE-100 44 Stockholm, Sweden*⁵*Condensed Matter Theory Group, Department of Physics, Uppsala University, Uppsala Box 530, Sweden*

(Received 4 March 2011; revised manuscript received 9 May 2011; published 10 August 2011)

The diffusion statistics of atoms in a crystal close to the critical superheating temperature was studied in detail using molecular dynamics and Monte Carlo simulations. We present a continuous random-walk model for diffusion of atoms hopping through thermal vacancies. The results obtained from our model suggest that the limit of superheating is precisely the temperature for which dynamic percolation happens at the time scale of a single individual jump. A possible connection between the critical superheating limit and the maximization of the Shannon entropy associated with the distribution of jumps is suggested. As a practical application of our results, we show that an extrapolation of the critical superheating temperature (and therefore an estimation of the melting point) can be performed using only the dynamical properties of the solid state.

DOI: [10.1103/PhysRevB.84.064102](https://doi.org/10.1103/PhysRevB.84.064102)

PACS number(s): 64.70.dm, 61.72.jd, 66.30.-h, 64.60.ah

I. INTRODUCTION

While it is a fairly common phenomenon in daily life, the complexity of the solid-liquid phase transition (melting) at the atomic level is such that a precise physical explanation of its nature and, in particular, its dynamics, is still lacking. Under special conditions, it is possible to overheat a solid (in an homogeneous way) above its melting point T_m , but there is a critical temperature, the limit of superheating T_{LS} , above which melting is unavoidable. Thermodynamically, for isobaric melting, T_m is defined by $G_{\text{solid}}(T_m, P) = G_{\text{liquid}}(T_m, P)$, G being the Gibbs free energy. There is no such clear definition for T_{LS} yet.

Besides the well-known Lindemann¹ and Born² criteria for melting, a number of additional criteria have been suggested, as an attempt to understand either T_{LS} or T_m and relate them to some qualitative change in the properties of the crystal. It seems, however, that the fulfillment of these classical criteria is preceded by local nucleation of liquid, as has been put into evidence by recent simulation studies.^{3,4}

In 1979, Cotterill⁵ suggested, from simulations of the Lennard-Jones liquid, that vacancies do not play any important role in melting, due to the lack of enough density inhomogeneities found in that state. This, however, does not rule out the presence of thermal vacancies in the superheated phase. Nordlund and Averback⁶ focused on self-interstitials and Frenkel pairs instead, finding that their concentration is higher than expected near melting, a fact that provides an explanation for the anomalous (non-Arrhenius) diffusion in superheated Cu crystals. Recently, similar studies have been performed by Forsblom *et al.*,^{7,8} finding that melting is initiated by a few interstitials and/or vacancies.

Burakovsky and co-workers^{9,10} have postulated a model that treats dislocations, in the form of closed noninteracting loops, as the central element in the study of melting. Their model suggests the transition from an ideal solid to an intermediate phase, a highly dislocated solid, as the precursor to melting.

Recently, Wang¹¹ introduced a model where there is a critical concentration of mobile atoms triggering a local instability in the crystal, and this model agrees with their homogeneous nucleation catastrophe model.³ Delogu^{12–14} characterizes the generation of atoms with defective coordination close to the melting point, atoms that tend to form extended, stringlike clusters. Atomic movement along these defect lines provides a potential mechanism for augmented self-diffusion, which is similar to the scenario presented by Nordlund in terms of self-interstitials.

Our previous results on superheated solids at constant energy¹⁵ seem to rule out the accumulation of defective or liquidlike atoms before melting. Instead, the concentration of defects suddenly increases at the instant melting is triggered. Bai *et al.*¹⁶ compared isothermal melting and “catastrophic melting” (induced by a fast heating rate), and found a critical concentration of self-diffusion loops (which are not dislocation loops), which induces melting.

It has been shown,¹⁷ using thermodynamic considerations, that T_{LS} is closely connected to the melting point itself, namely that the ratio T_{LS}/T_m tends to $1 + \frac{1}{3} \ln 2$ in the limit of high pressures for monatomic solids. Thus understanding the behavior at the superheating limit might shed some light on the mechanism of melting. Besides this connection and all the previously suggested scenarios, the origin and the nature of the superheating limit itself is far from clear. We are certain that some mechanism for augmented diffusion (be it through thermal defects or dislocation loops) right before melting or at the limit of superheating plays a central role in this transition. It is also known that the population of such defects increases as we get closer to T_{LS} . But, can some qualitative change in the behavior of thermal defects be ascribed as the meaning of T_{LS} ?

In this paper, we propose a continuous random-walk model, which is able to explain the behavior of the kind of diffusion seen in a superheated solid. Our model suggests that, in fact, the superheating limit might be defined as the temperature for

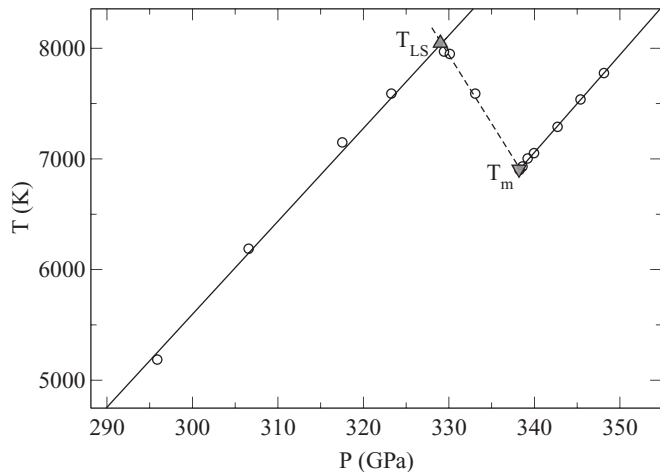


FIG. 1. Example of the application of the Z method to determine the melting temperature. The relation between T_m (lower point of the Z-shaped isochoric curve) and T_{LS} (higher point) is shown for an embedded atom solid.

which the dynamic percolation threshold coincides with the time scale of a single individual jump.

II. THE NEED FOR MICROCANONICAL SIMULATIONS OF SUPERHEATING: THE Z METHOD

A recent approach to determining the melting point using molecular dynamics (MD) is the Z method,¹⁷ which does not require the simulation of a coexistence between two phases, being in fact a one-phase method. Instead, the idea is to perform microcanonical ensemble (constant total energy, constant volume, and number of atoms) simulations on a single solid system at different total energies to reach a realistic T_{LS} , without any external intervention on the natural dynamics of the melting process (due, for example, to “thermostat algorithms” used to constrain temperature). A system being simulated in the microcanonical ensemble slightly above T_{LS} will eventually melt, its temperature dropping spontaneously to the melting point T_m corresponding to the pressure conditions imposed by the chosen density.

At a fixed volume, the (P, T) points of the isochoric curve draw a “Z” shape (hence the name of the method), like the one shown in Fig. 1. In this Z-shaped curve, the sharp inflection at the higher temperature corresponds to T_{LS} and the one at the lower temperature to T_m .

III. SUPERDIFFUSIVE BEHAVIOR AT T_{LS}

For the liquid state, it is usual to compute the mean-square displacement (MSD) of the atoms as a function of time,

$$\langle r(\tau)^2 \rangle = \langle [\vec{r}(t_o + \tau) - \vec{r}(t_o)]^2 \rangle, \quad (1)$$

where the average on the right-hand side is taken over all atoms and all origins of time t_o . In a liquid, the MSD is linear with time and the diffusion coefficient D comes directly from

$$\langle r(\tau)^2 \rangle = 2dD\tau, \quad (2)$$

where d is the dimensionality of the system.

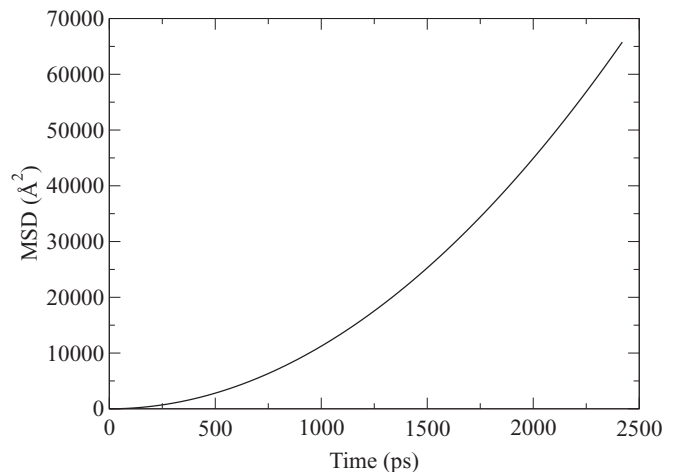


FIG. 2. Mean-square displacement for a time interval up to 2.5 ns, computed for the EAM solid at $T = 7000 \text{ K} = 0.75T_{LS}$.

An advantage of the Z method over canonical (“thermostatted”) melting simulations is that we can sample the unperturbed dynamics of the atoms just before melting is triggered, and then it is possible to compute the MSD for the superheated solid.

In the following, we describe the results of Z-method simulations using both a Lennard-Jones (LJ) solid and an embedded atom model (EAM) solid. Molecular-dynamics simulations were performed in both cases using the DLPOLY¹⁸ and LPMD¹⁹ software packages. All the post analysis of the simulation data, including computation of structural and dynamical properties, was performed using LPMD.

At temperatures between T_m and T_{LS} , we have observed a superdiffusive regime, characterized by a mean-square displacement $\langle r^2(\tau) \rangle$ that follows a power law,

$$\langle r^2(\tau) \rangle \propto \tau^\gamma, \quad (3)$$

with $1 < \gamma < 2$. Figure 2 shows $\langle r^2 \rangle$ at a temperature near 75% of the superheating limit, while Fig. 3 shows the dependence of the exponent γ with the normalized temperature, T/T_{LS} .

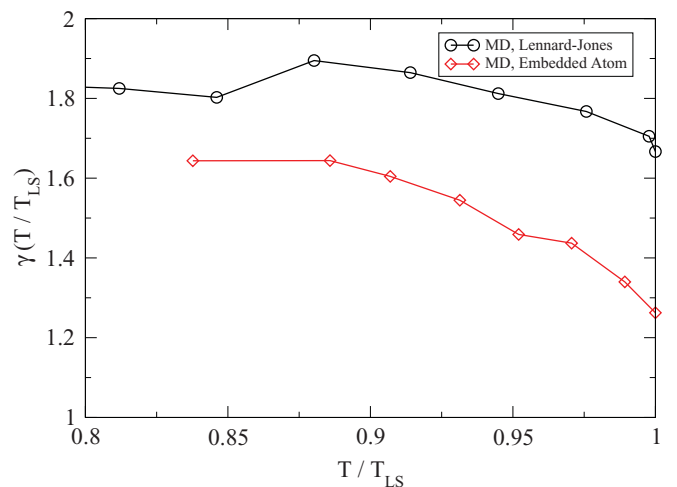


FIG. 3. (Color online) Mean-square displacement exponent γ as a function of temperature for the LJ and EAM solids.

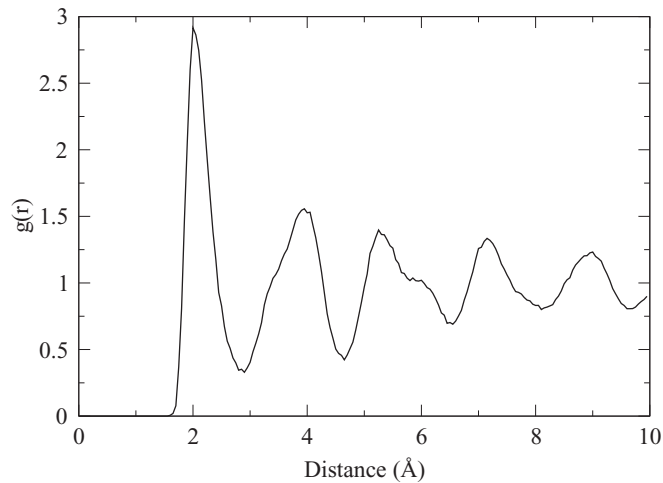


FIG. 4. Average radial distribution function $g(r)$ computed for the EAM solid at $T = 7000 \text{ K} = 0.75T_{LS}$.

We can see that even in the time scale of nanoseconds, there is anomalous diffusive behavior, different from the usual $\gamma = 1$ expected in a three-dimensional, unbiased random walk over arbitrary points in space. In fact, in this case we see a value of γ equal to 1.98. Figure 4 shows the average radial distribution function corresponding to the same conditions, which confirms that the system still has a definite solid structure (note the “shoulders” near 3.5, 5.5, and 7.5 Å), despite the superdiffusive behavior.

It can be shown²⁰ that, for a random walk having variable step vectors $\Delta\vec{r}$, the MSD is given by

$$\langle r(\tau)^2 \rangle = (\omega_j \tau)^2 \langle |\Delta\vec{r}|^2 \rangle + (\omega_j \tau) \langle |\Delta\vec{r}|^2 \rangle, \quad (4)$$

where ω_j is the frequency of jumps. This shows explicitly that asymmetrical jumps ($|\langle \Delta\vec{r} \rangle| \neq 0$) are needed to obtain the superdiffusive behavior. This implies a biased random walk.

Dealing with the possibility that the anomalous diffusion (and the implied biased random walk) could be just an artifact of the microcanonical MD simulations, we have performed also microcanonical Monte Carlo (MC) simulations on the same system, using the algorithm by Creutz.²¹ Figure 5

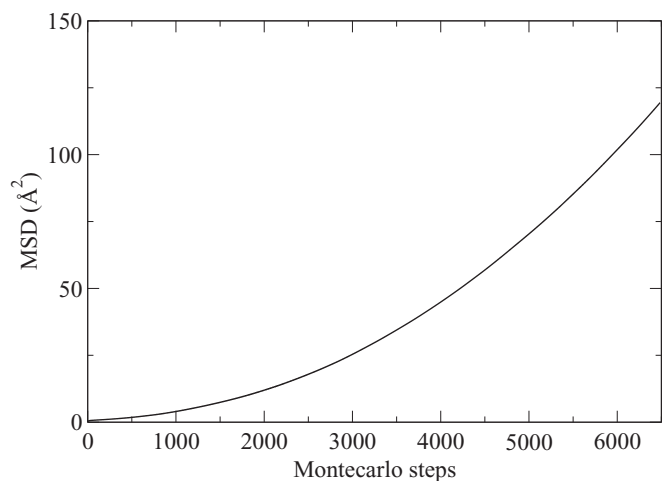


FIG. 5. Mean-square displacement computed for the LJ solid at $T = 6200 \text{ K} = 0.99T_{LS}$ with Creutz’s microcanonical MC algorithm.

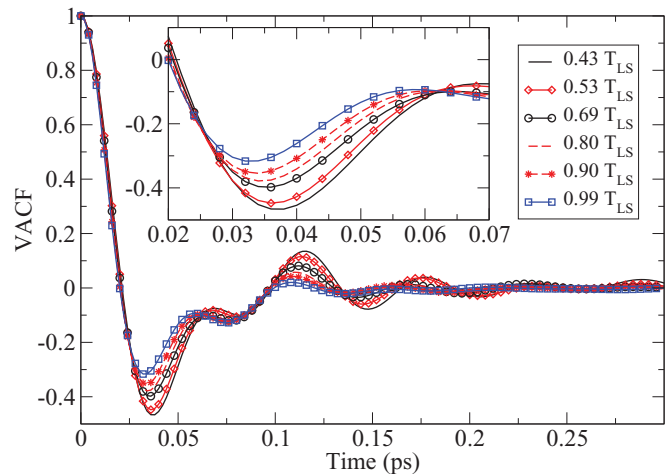


FIG. 6. (Color online) Velocity autocorrelation function (VACF) for different temperatures approaching the superheating limit T_{LS} . The inset shows the time scale corresponding to atomic vibrations.

shows the mean-square displacement near T_{LS} , which again is superdiffusive.

An explanation of the observed superdiffusion on the mostly crystalline solid at T_{LS} should involve the explicit modeling of thermal defects and the “hopping” processes they activate. A similar observation of the importance of these isolated thermal defects (instead of whole nucleation processes, as observed in canonical MD simulations) has been reported by Wang *et al.*,¹¹ Delogu,^{12–14} and recently by Gallington *et al.*²²

To complete the picture about dynamical properties of a superheated solid, the velocity autocorrelation function (VACF) and vibrational density of states (vDOS) were computed for different temperatures close to T_{LS} and also for a liquid sample. The results are shown in Figs. 6 and 7. Figure 8 shows a comparison of these properties for the superheated and liquid state. Not much of a qualitative difference is seen as temperature increases. The only noticeable aspect is the appearance of the zero-frequency component in the liquid vDOS (Fig. 8), which is related to Brownian ($\gamma = 1$) self-diffusion.

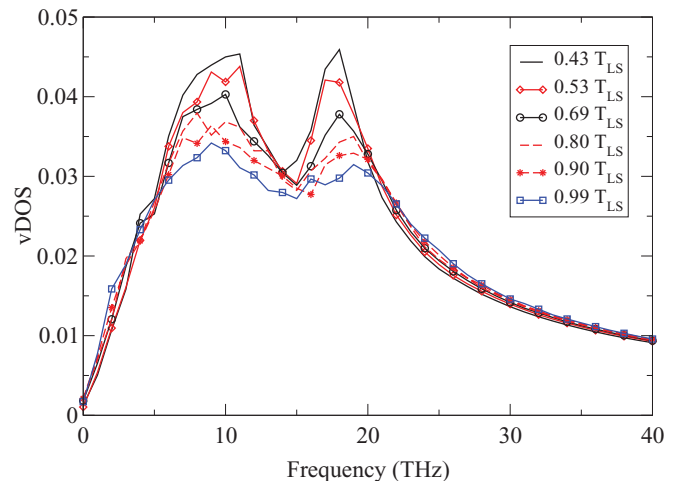


FIG. 7. (Color online) Vibrational density of states for different temperatures approaching the superheating limit T_{LS} .

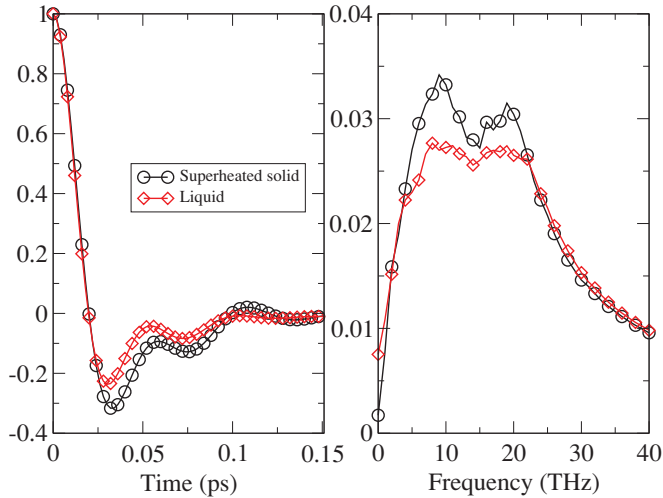


FIG. 8. (Color online) Comparison between superheated and liquid vibrational properties. Left, velocity autocorrelation function. Right, vibrational density of states.

IV. A MODEL FOR DIFFUSION

The analysis of the MSD is useful to get an overall view of the diffusive properties of the system, but it does not give any details about the diffusivity of individual atoms, or the statistical distribution behind the MSD average.

For this purpose, we can define the probability distribution of displacements $J(r, \tau)$ as the number of atoms traveling a distance between r and $r + \Delta r$ in a time interval τ . The MSD can be obtained as the expectation value of r^2 under the probability distribution J , i.e.,

$$\langle r(\tau)^2 \rangle = E_J(r^2) = \int_0^\infty r^2 J(r, \tau) dr. \quad (5)$$

For the sake of brevity, we shall refer to the function $J(r)$ [i.e., $J(r, \tau)$ taken at a constant τ] as the mobility histogram of the system for the given observation interval τ . An example of such a histogram for two different temperatures in a solid close to $T_{LS} = 8000$ K is shown in Fig. 9. Note the decrease in the height of the first peak ($r/r_0 < 0.5$) and the corresponding increase in heights for the second ($0.5 < r/r_0 < 1.5$) and third ($r/r_0 > 1.5$) peaks at increasing temperature.

Considering a fixed observation interval τ , we can roughly classify the population of atoms into three kinds: atoms with displacement around zero, atoms with displacement around the nearest-neighbor distance r_0 , and atoms with displacement larger than r_0 . These three kinds of atoms will have fractional populations J_0 , J_1 , and J_r , such that

$$J_0 + J_1 + J_r = 1. \quad (6)$$

These fractional populations (or mobility components) can be obtained from $J(r, \tau)$ by taking the integral over r ,

$$J_0(\tau) = \frac{1}{N} \int_0^{\rho_0} J(r, \tau) dr, \quad (7)$$

$$J_1(\tau) = \frac{1}{N} \int_{\rho_0}^{\rho_1} J(r, \tau) dr, \quad (8)$$

$$J_r(\tau) = \frac{1}{N} \int_{\rho_1}^\infty J(r, \tau) dr, \quad (9)$$

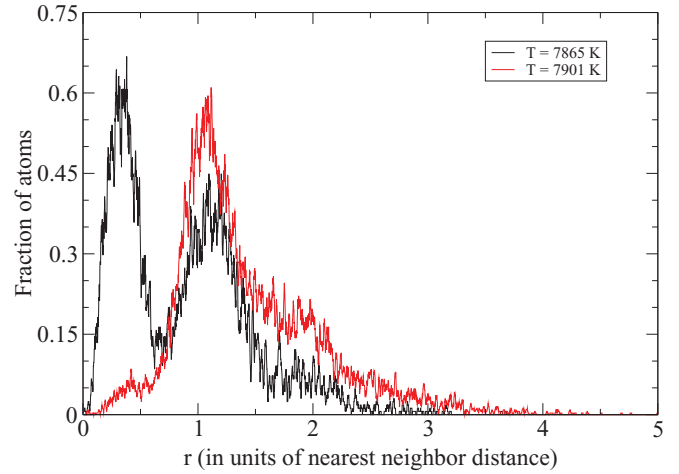


FIG. 9. (Color online) Mobility histograms $J_\tau(r)$ obtained from molecular-dynamics simulations of an EAM solid close to T_{LS} .

where ρ_0 is taken as the minimum distance between atoms (due to repulsion) and ρ_1 is taken as slightly higher than r_0 , in order to include the whole first-neighbor shell. In practice, both radii can be obtained from the radial distribution function (RDF).

For an ideal solid without defects, the only displacement of the atoms is due to thermal vibrations around their equilibrium positions. In this case, $J_0(\tau) = 1$. If we consider thermal defects, depending on the observation time τ , some atoms will jump to the nearest vacant site, or even jump further away through a series of jumps. Those “diffusive” atoms will contribute to J_1 and J_r at the expense of decreasing J_0 , the fraction of “nondiffusive” atoms.

Taking this into account, it is clear that the mobility histogram (and its components J_0 , J_1 , and J_r) will be highly dependent on the number of vacant sites f available to jump, which in the case of a finite-temperature crystal corresponds to the equilibrium fraction of thermal vacancies,²³

$$f = e^{-E_v/k_B T}, \quad (10)$$

where E_v is the energy needed to create a vacancy-interstitial pair in the crystal.

It will also be dependent on the average number of successful jumps n_j performed during the time interval τ . This in turn is given by the probability of jumping P_j , as $n_j = P_j(\tau/\tau_j)$, where τ_j is the average time it takes an atom to jump.

In a finite-temperature crystal, P_j is also given by a Boltzmann factor,

$$P_j = e^{-E_j/k_B T}, \quad (11)$$

where E_j is the energy barrier the atom has to cross to jump into a neighboring vacant site.

If we consider the effects of temperature only through $f(T)$ and $P_j(T)$, we can reduce the problem of studying the statistics of diffusion in a crystal with defects to a discrete mathematical problem of a random walk over a percolation lattice (i.e., a lattice where sites are connected with “open” and “closed” bonds²⁰). However, as the distribution of open and closed bonds (determined by the particular spatial distribution of thermal vacancies) is not static, but is in fact renewed with

a certain frequency (lower than the frequency of jumping), we should speak instead of a dynamic percolation problem.²⁴⁻²⁸

V. MATHEMATICAL DESCRIPTION OF THE RANDOM WALK ON A LATTICE

The simpler problem of an isotropic random walk over a lattice is fully described by the probability of reaching a given lattice point \vec{r} , starting from the origin, in n steps. This probability, denoted as $P_n(\vec{r})$, can be obtained from the ordinary generating function

$$P(\vec{r}; z) = \sum_{n=0}^{\infty} P_n(\vec{r}) z^n, \quad (12)$$

called the lattice Green's function at the lattice point \vec{r} . For a given lattice, $P(\vec{r}; z)$ can be computed as²⁰

$$P(\vec{r}; z) = \frac{1}{(2\pi)^d} \int_B \frac{e^{-i\vec{k}\cdot\vec{r}}}{1 - z\lambda(\vec{k})} d\vec{k}, \quad (13)$$

where $\lambda(\vec{k})$ is the structure function for the lattice, and the integration is performed over the first Brillouin zone, d being the dimensionality of the lattice.

The structure function $\lambda(\vec{k})$ includes the probability of jumping to the different sites from the origin, and is defined as

$$\lambda(\vec{k}) = \sum_i e^{i\vec{k}\cdot\vec{R}_i} p(\vec{R}_i), \quad (14)$$

where the summation is performed over all the allowed jump displacements \vec{R}_i from the origin, and $p(\vec{r})$ is the probability associated with the displacement \vec{r} .

If we assume the jump events follow a Poisson distribution in time, with the average number of jumps in a time interval τ given by

$$\langle n(\tau) \rangle = \frac{P_j \tau}{\tau_j}, \quad (15)$$

we can obtain a model for a continuous-time random walk on a lattice, which will be characterized by the Poisson generating function,

$$G(\vec{r}; \tau) = \sum_{n=0}^{\infty} P_n(\vec{r}) \frac{(P_j \tau / \tau_j)^n}{n!} e^{-P_j \tau / \tau_j}. \quad (16)$$

This function gives directly the probability of reaching a lattice point \vec{r} from the origin in a time interval τ .

From the series expansion of the $\frac{1}{1-z\lambda(\vec{k})}$ factor in Eq. (13) and comparing with Eq. (12), we can obtain the series coefficient

$$P_n(\vec{r}) = \frac{1}{(2\pi)^d} \int_B \lambda^n(\vec{k}) e^{-i\vec{k}\cdot\vec{r}} d\vec{k}. \quad (17)$$

Including this into the Poisson generating function in Eq. (16), we have

$$G(\vec{r}; \tau) = \frac{e^{-P_j \tau / \tau_j}}{(2\pi)^d} \int_B e^{-i\vec{k}\cdot\vec{r} + (P_j \tau / \tau_j) \lambda(\vec{k})} d\vec{k}. \quad (18)$$

From $G(\vec{r}; \tau)$ we can obtain the mobility components as

$$J_0(\tau) = G(\vec{0}; \tau), \quad (19)$$

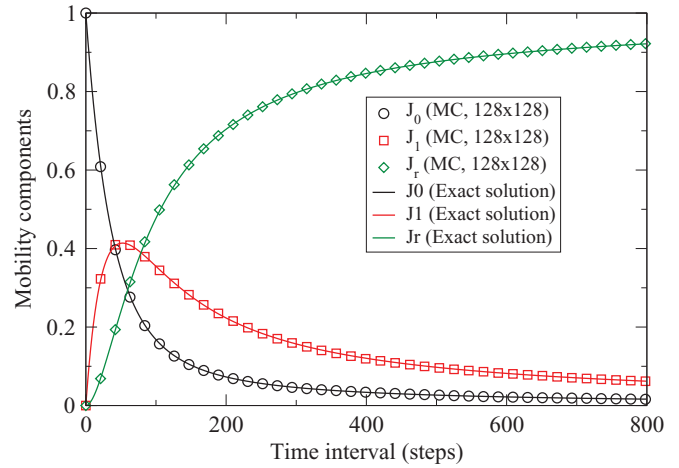


FIG. 10. (Color online) Mobility components for the simple random walk in a square lattice.

$$J_1(\tau) = \sum_{i=1}^{n_c} G(\vec{R}_i; \tau), \quad (20)$$

$$J_r(\tau) = 1 - J_0(\tau) - J_1(\tau), \quad (21)$$

with n_c the coordination number of the lattice. For the simple case of the square lattice, Eq. (18) can be evaluated exactly at the origin and over the first neighbors. Then J_0 and J_1 can be obtained as

$$J_0(\tau) = e^{-P_j \tau / \tau_j} I_0^2 \left(\frac{P_j \tau}{2\tau_j} \right), \quad (22)$$

$$J_1(\tau) = 4e^{-P_j \tau / \tau_j} I_0 \left(\frac{P_j \tau}{2\tau_j} \right) I_1 \left(\frac{P_j \tau}{2\tau_j} \right), \quad (23)$$

where the $I_k(x)$ are the modified Bessel functions of the first kind.

Figure 10 shows the mobility components obtained from MC simulations of the isotropic random walk in a square lattice, compared to the exact solutions [Eqs. (22) and (23)]. The observed agreement validates the MC simulations and the assumption of Poisson statistics for the jump events.

These mobility curves can be interpreted as follows: increasing the observation interval τ leads to a monotonic decrease in the population of nondiffusive atoms (J_0), together with an, also monotonic, increase in the population of long-range diffusive atoms (J_r). However, J_1 , the population of atoms sitting one nearest-neighbor distance from their equilibrium positions, reaches a maximum value J_c and then decreases. This marks out two regimes, one where the atoms mainly hop following closed paths, quickly returning to their starting positions (recurrent random-walk states), and another where the atoms wander far away following open paths, eventually percolating through the entire system if the observation interval is large enough (transient random-walk states).^{20,29}

This scenario is reminiscent of the picture proposed by Bai *et al.*,¹⁶ in which a critical concentration of self-diffusion “loops” (either open or closed) triggers melting. It is also compatible with the picture by Delogu,¹² characterized by pairs of atoms having defective coordination that form extended “channels” (compare with Bai’s open loops) enabling

self-diffusion. Their MD simulations, however, were performed under NPT (constant pressure, constant temperature) conditions, so despite the qualitative similarity of the picture, it is difficult to compare quantitatively to our results in terms of mobility histograms.

Another alternative scenario involves the formation of dislocation lines just before melting.^{9,10} Our previous simulations of superheating in the microcanonical ensemble¹⁵ revealed that defective atoms just before melting are relatively scarce and spatially isolated, a picture that is different from the one expected in the case of dislocation lines. This disagreement with the recent evidence for dislocations as a precursor of melting is just apparent, as, again, they discuss the initiation of melting in the canonical ensemble, under a much lower T_{LS} than ours and, therefore, under conditions where more complex, higher-energy defects are allowed to form. In our case, at such high T_{LS} , a single open loop percolating through the system might be enough to initiate melting.

From the curves in Fig. 10, we can define two characteristic observation intervals, or *crossing times*, τ_0 and τ_1 , such that

$$J_0(\tau_0) = J_r(\tau_0), \quad (24)$$

$$J_0(\tau_1) = J_1(\tau_1). \quad (25)$$

The crossing time τ_1 is the average time interval needed to observe a single jump. It only depends on the frequency of attempts to jump τ_j^{-1} and the probability of jumping P_j . The crossing time τ_0 is the average time interval needed to jump beyond the first-neighbor shell. So, for $\tau < \tau_1$, the atoms are just oscillating around their equilibrium positions; for $\tau_1 < \tau < \tau_0$, the atoms are mostly jumping back and forth; and for $\tau > \tau_0$, the atoms are diffusing away from their starting positions.

VI. MONTE CARLO SIMULATIONS

The presence of vacancies mediating the jumps can be included by modifying the structure function $\lambda(\vec{k})$ to include a finite probability to jump, which will depend on the availability of vacancies around the starting point,

$$\lambda'(\vec{k}; f) = \sum_i e^{i\vec{k}\cdot\vec{R}_i} F(f; n_c) p(\vec{R}_i) = F(f; n_c) \lambda(\vec{k}), \quad (26)$$

where $F(f; n_c)$ represents the probability of having at least one available neighbor vacancy to jump into. We can model F under the Ansatz

$$F(f; n_c) \approx 1 - e^{-fn_c},$$

which comes from assuming that, around each atom, vacancies are Poisson-distributed with average number fn_c .

In this way, the new Poisson generating function $G(\vec{r}; \tau, f)$ can be expressed as

$$G(\vec{r}; \tau, f) = \frac{e^{-P_j\tau/\tau_j}}{(2\pi)^d} \int_B e^{-i\vec{k}\cdot\vec{r} + \frac{P_j\tau F(f; n_c)}{\tau_j} \lambda(\vec{k})} d\vec{k}, \quad (27)$$

and the mobility components as simple corrections over Eqs. (22) and (23),

$$J_0(\tau; f) = e^{-P_j\tau/\tau_j} I_0^2 \left(\frac{P_j\tau F(f; n_c)}{2\tau_j} \right), \quad (28)$$

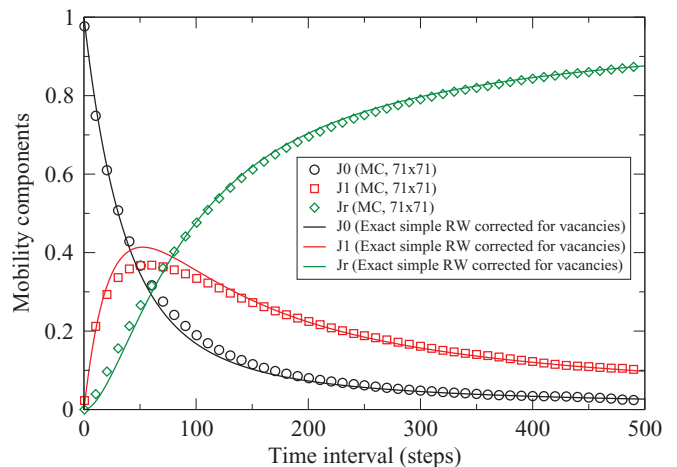


FIG. 11. (Color online) Mobility components for the vacancy-mediated random walk in a square lattice.

$$J_1(\tau; f) = n_c e^{-P_j\tau/\tau_j} I_0 \left(\frac{P_j\tau F(f; n_c)}{2\tau_j} \right) I_1 \left(\frac{P_j\tau F(f; n_c)}{2\tau_j} \right). \quad (29)$$

To confirm the validity of this expression, we performed MC simulations of the discrete vacancy-driven random walk on a lattice.

In this approach, the system consists of a lattice of N points, where initially every point has a probability f of being an empty site (a vacancy) and $1 - f$ of being an occupied site (an atom). For the Markov chain, the move consists simply of attempting to exchange a vacancy with an occupied site, with probability P_j . In this way, the total number of vacancies Nf is kept constant during the simulation. Figure 11 plots Eqs. (28) and (29) against the results from MC simulations of the square lattice. There is an overall agreement, except for small deviations around the maximum of J_1 , precisely the region where open paths become important.

Tables I and II show the values of the maximum height of $J_1(\tau)$, denoted by J_c , obtained from MC simulations for three-dimensional and two-dimensional lattices, respectively.

It is interesting to note that J_c for ideal structures seems to have only two possible values: either close to 0.46 for the close-packed structures [fcc and hcp structures in three dimensions (3D), hexagonal structure in two dimensions (2D)] or close to 0.38 for the loose-packed ones.

The explanation for this discrete behavior of J_c could be related to the enumeration of closed jump paths²⁰ implicit in $P_n(\vec{0})$. For a loose-packed structure, there is no closed graph on the lattice with an odd number of edges. However, for a

TABLE I. J_c versus coordination number n_c , obtained from MC simulations for several 3D lattices.

Structure	n_c	J_c
sc	6	0.38385
bcc	8	0.38645
fcc	12	0.46082
hcp	12	0.45791

TABLE II. J_c versus coordination number n_c obtained from MC simulations for several 2D lattices.

Structure	n_c	J_c
Honeycomb	3	0.38738
Square	4	0.37771
Hexagonal	6	0.46132

closed-packed structure, there are closed graphs with an odd and even number of edges. The number of closed graphs is directly related to $J_0(\tau)$ and also indirectly to $J_1(\tau)$, because every n -step random-walk trajectory contributing to J_1 can be mapped to an $(n+1)$ -step closed trajectory (by adding the edge that closes the loop).

To see that our discrete-jump model captures the essence of the dynamics of the crystal, we compare the mobility components for MC simulations of an ideal fcc structure with molecular-dynamics simulations of a Lennard-Jones solid. The results are shown in Fig. 12.

In terms of the finite-temperature crystal, as temperature increases, both f and P_j will increase as well, according to Eqs. (10) and (11). Eventually the concentration of thermal defects and the rate of barrier crossing events will be high enough that the system will cross its dynamic percolation threshold τ_0 , the population J_r overcoming J_0 . Given that the spatial distribution of vacancies and atoms changes over time, it is possible to achieve percolation even when the concentration of vacancies is less than the “static” site percolation threshold.^{30,31}

To study the connection of this kind of diffusion with the superheating limit, we have computed the temporal evolution of J_0 , J_1 , and J_r , as well as the exponent γ , during several MD simulations at increasing temperatures, near T_{LS} . The mobility components are shown in Fig. 13 for the case in which the crystal melts, and Fig. 3 shows the thermal dependence of γ .

We can see that, according to the drop in instantaneous temperature, the instant when melting is triggered corresponds

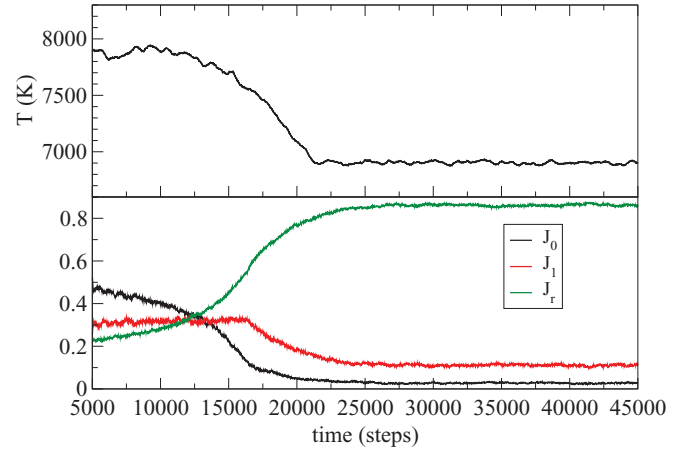


FIG. 13. (Color online) (a) Instantaneous temperature as a function of time during melting. (b) Jump diffusion components as a function of time.

precisely to the crossing of J_0 and J_r . This is valid for every observation interval τ large enough to see contributions to J_1 .

VII. CONNECTION BETWEEN T_{LS} AND THE MOBILITY COMPONENTS

From MD simulations at T_{LS} , we note that the mobility curves J_0 , J_1 , and J_r always seem to cross at the same time interval $\tau_D = \tau_0 = \tau_1$, whereas for T above or below T_{LS} there is a clear separation between the different diffusion time scales τ_0 and τ_1 . This is shown in Fig. 14.

The behavior of τ_0 and τ_1 with increasing temperature is shown in Fig. 15. It is clear that, as one approaches T_{LS} , not only does τ_0 decrease, but it becomes closer and closer to τ_1 . Eventually at $T = T_{LS}$ we have $\tau_0 = \tau_1 = \tau_D$, and then

$$J_0(\tau_D) = J_1(\tau_D) = J_r(\tau_D) = \frac{1}{3}. \quad (30)$$

This “collapse” of the three J_i curves to $1/3$ does not arise from our simple geometric MC model, as in this model

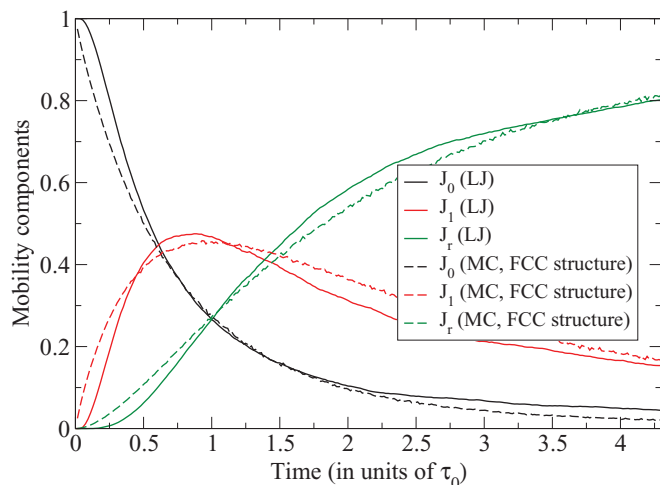


FIG. 12. (Color online) Comparison between the J_i curves as a function of observation time for Lennard-Jones MD (Ar, 108 atoms) and the MC geometrical model.

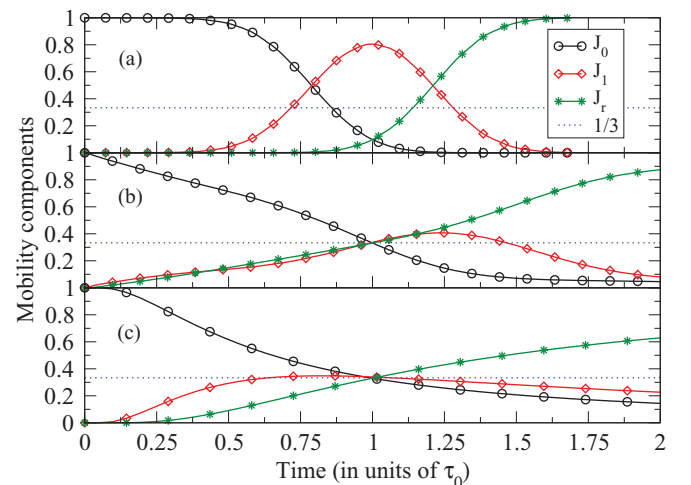


FIG. 14. (Color online) Mobility components computed from MD simulations as a function of the normalized observation time τ/τ_0 , (a) at $T < T_{LS}$ in the solid isochore, (b) at T_{LS} , and (c) in the liquid isochore. The dotted line $J = 1/3$ is drawn for clarity.

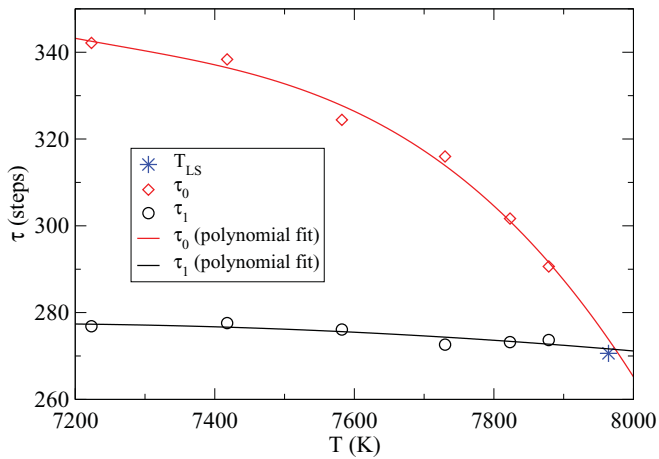


FIG. 15. (Color online) Characteristic observation times τ_0 and τ_1 on increasing temperatures, close to T_{LS} . The star corresponds to the measured T_{LS} and $\tau = \tau_D$.

the positions on the crystal lattice are fixed; only exchanges between atoms and vacancies are allowed as moves in the Markov chain process. In that case, $J_c = J_1(\tau_0)$ is always close to either 0.38 (for loose-packed structures) or 0.46 (for close-packed ones). We know from the MC model that J_c is directly related to the distribution of closed random-walk paths, therefore the fact that J_c tends to 1/3 at T_{LS} in MD simulations seems to suggest that the crystal becomes even less packed (in terms of the possible closed trajectories) than the original structure just prior to melting.

Interestingly, one could also speculate that the collapse of the J_i curves corresponds to the maximization of the Shannon

entropy associated to $J(r, \tau_D)$,

$$S_J = - \int_0^\infty J(r, \tau_D) \ln J(r, \tau_D) dr, \quad (31)$$

because, at this point, it is equally probable for a given atom to be in any of the three diffusion populations: J_0 , J_1 , or J_r . This hypothesis and its implications remain to be explored.

VIII. CONCLUSIONS

We have developed and tested a model to explain jump-mediated diffusion due to thermal vacancies near T_{LS} and its role in defining it. The application of our model to MD simulations suggests that T_{LS} is the temperature at which the change in diffusion behavior, from recurrent random walks to transient random walks, takes place at a particular time scale τ_D , which can be determined solely from the mobility of the atoms in the solid phase. A possible connection between the critical superheating limit and the maximization of the Shannon entropy associated with the mobility histogram $J(r)$ is suggested.

ACKNOWLEDGMENTS

Computations were performed at the National Supercomputer Center (NSC) in Linköping and the Parallel Computer Center (PDC) in Stockholm. We also thank the Swedish Research Council VR for financial support, and S.D. acknowledges partial support from Fondecyt 3110017. S.D. wishes to thank Gonzalo Gutiérrez and Jaime Roessler for enlightening discussions.

¹F. A. Lindemann, *Z. Phys. Chem., Stoichiom. Verwandtschaftsl.* **11**, 609 (1910).
²M. Born, *J. Chem. Phys.* **7**, 591 (1939).
³K. Lu and Y. Li, *Phys. Rev. Lett.* **80**, 4474 (1998).
⁴Z. H. Jin, P. Gumbsch, K. Lu, and E. Ma, *Phys. Rev. Lett.* **87**, 055703 (2001).
⁵R. M. J. Cotterill, *Phys. Rev. Lett.* **42**, 1541 (1979).
⁶K. Nordlund and R. S. Averback, *Phys. Rev. Lett.* **80**, 4201 (1998).
⁷M. Forsblom and G. Grimvall, *Nat. Mater.* **4**, 388 (2005).
⁸M. Forsblom and G. Grimvall, *Phys. Rev. B* **72**, 054107 (2005).
⁹L. Burakovsky, D. L. Preston, and R. R. Silbar, *Phys. Rev. B* **61**, 15011 (2000).
¹⁰L. Gómez, A. Dobry, C. Geuting, H. T. Diep, and L. Burakovsky, *Phys. Rev. Lett.* **90**, 095701 (2003).
¹¹L. W. Wang, L. Zhang, and K. Lu, *Philos. Mag. Lett.* **85**, 213 (2005).
¹²F. Delogu, *J. Phys. Chem. B* **109**, 15291 (2005).
¹³F. Delogu, *J. Phys. Chem. B* **110**, 12645 (2006).
¹⁴F. Delogu, *Phys. Rev. B* **73**, 184108 (2006).
¹⁵A. B. Belonoshko, S. Davis, N. V. Skorodumova, P. H. Lundow, A. Rosengren, and B. Johansson, *Phys. Rev. B* **76**, 064121 (2007).
¹⁶X. M. Bai and M. Li, *Phys. Rev. B* **77**, 134109 (2008).
¹⁷A. B. Belonoshko, N. V. Skorodumova, A. Rosengren, and B. Johansson, *Phys. Rev. B* **73**, 012201 (2006).

¹⁸W. Smith, dLPOLY 3, release 3.06 (2006).
¹⁹S. Davis, C. Loyola, F. González, and J. Peralta, *Comput. Phys. Commun.* **181**, 2126 (2010).
²⁰B. D. Hughes, *Random Walks and Random Environments* (Clarendon, Oxford, 1995).
²¹M. Creutz, *Phys. Rev. Lett.* **50**, 1411 (1983).
²²L. C. Gallington and A. Bongiorno, *J. Chem. Phys.* **132**, 174707 (2010).
²³M. Hillert, *Phase Equilibria, Phase Diagrams and Phase Transformations* (Cambridge University Press, 1998).
²⁴S. D. Druger, A. Nitzan, and M. A. Ratner, *J. Chem. Phys.* **79**, 3133 (1983).
²⁵S. D. Druger, M. A. Ratner, and A. Nitzan, *Phys. Rev. B* **31**, 3939 (1985).
²⁶R. Granek and A. Nitzan, *J. Chem. Phys.* **92**, 1329 (1990).
²⁷A. P. Chatterjee and R. F. Loring, *Phys. Rev. E* **50**, 2439 (1994).
²⁸O. Bénichou, J. Klafter, M. Moreau, and G. Oshanin, *Phys. Rev. E* **62**, 3327 (2000).
²⁹F. Spitzer, *Principles of Random Walk* (Springer, 2001).
³⁰G. Grimmett, *Percolation* (Springer-Verlag, Berlin, 1989).
³¹D. Stauffer and A. Aharony, *Introduction to Percolation Theory* (CRC, Boca Raton, FL, 1994).